Journal of Radioanalytical and Nuclear Chemistry (2022) 331:4587–4600
https://doi.org/10.1007/s10967-022-08529-1

Effects of dry processing on adsorption of uranium on Mg-Al layered double hydroxides and calcined layered double oxides

qinqin Tao[1] · Jinhua Xie[1] · Yan Li[1] · Ying Dai[1,2,3] · Zhirong Liu[1,2,3]

Received: 16 June 2022 / Accepted: 29 August 2022 / Published online: 16 September 2022

Abstract

Mg-Al layered double hydroxides (LDH) (F-MgAl-LDHs and O-MgAl-LDHs) and Mg-Al layered double oxides (LDO) (F-MgAl-LDO and O-MgAl-LDO) nanosheets were prepared using a modified co-precipitation and oven/freeze dry route for adsorption of uranium. The freeze dry could evidently promote the adsorption ability. It's resulted from larger specific surface (F-MgAl-LDO > F-MgAl-LDHs > O-MgAl-LDO > O-MgAl-LDHs) and pore size, as well as sufficient expose of vacant sites in the inner struture of F-MgAl-LDHs and F-MgAl-LDO. The pH, shaking time, initial uranium concentation and temperature influenced the adsorption capacity of F-MgAl-LDHs, O-MgAl-LDHs, F-MgAl-LDO and O-MgAl-LDO, while ionic strength exerted slightly little influence. Na_2CO_3 highlighted the best desorption effectivity, with desorption efficiency of 97.84% for F-MgAl-LDHs and 98.52% for F-MgAl-LDO, respectively. It is noteworthy that maximum adsorption capacity of F-MgAl-LDO reached 1099.93 mg/g, locating the top rank in the uranium-specific adsorbents. The adsorption conformed to the pseudo-second-order model, indicating chemical adsorption in nature. The thermodynamic was also investigated. The adsorption mechanism was determined that M-O and C-O bonds participated the complex process in the uranium adsorption. The study proposed the freeze dry as an efficient method to promote adsorbent performance.

Keywords Freeze-dry processing · Layered bimetallic (hydrogen) oxides · Adsorption · Uranyl · Separation

Introduction

Uranium is a naturally-occurring actinides element, attracting huge attention since the utilization of nuclear energy. Due to extreme energy release via the fission reaction, uranium has been well known as a superior nuclear fuel [1]. Uranium of the hexavalent state is mainly in the formation of uranyl, which is highly mobile in aqueous environment [2]. Once enterring into human body, it would result in seriously irreversible injury because of heavy metal and radioactive toxicity. To avoid the potential risk, the US Environmental Protection Agency require the safe uranium concentration less than 20 μg/L [3]. To meet the requirement, treating uranium-containing wastwater is thus of significance before the discharge. Nowdays, the techniques solving heavy metal contamination mainly involve adsorption, solvent extraction, precipitation and membrane. Adsorption highlights feasibility, low secondary pollution and abundant adsorbents. Commonly used adsorbents include clay [4], metal oxide [5], polymer [6], and active char [7].

Layered double hydroxides (briefly as LDHs) is promising in the field of removal of heavy metal due to superior surface area, thermal stability and adjustable structure. Its chemical formula can be described as $[M^{2+}_{1-x}M^{3+}_{x}(OH)_2]^{x+}(A^{n-})_{x/n}{\cdot}mH_2O$ (M^{2+}, M^{3+} and A^{n-} mean divalent, trivalent cations and interlamination anions). In

✉ Ying Dai
daiying@ecut.edu.cn

✉ Zhirong Liu
199760011@ecut.edu.cn

1 State Key Laboratory of Nuclear Resources and Environment, East China University of Technology, 330013 Nanchang, P. R. China

2 Institute of Nuclear Agricultural Sciences, Key Laboratory of Nuclear Agricultural Sciences of Ministry of Agriculture and Zhejiang Province, Zhejiang University, 310058 Hangzhou, China

3 Jiangxi Province Key Laboratory of Polymer Micro/Nano Manufacturing and Devices, School of Chemistry, Biology and Materials Science, East China University of Technology, 330013 Nanchang, P. R. China

the past, most studies paid large attention to the removal performance for various anions [8] and organic molecules [9] of LDHs by taking advantage of hydrophilicity and exchangeable anion of LDHs. For example, Zubair et al. utilized biochar modified MgAl-LDH to adsorb an organic compound, methylene blue. The results proved the adsorption amount reached 302.75 mg/g [10]. Jung et al. found that Mg-Al layered double hydroxides-functionalized hydrochar composite possessed certain adsorption capacity toward anion, 16.222 mg/g for arsenate and 20.265 mg/g for phosphate [11]. Shi et al. used glycine-modified Fe/Cu-layered double hydroxides as a specific As(V) adsorbent. The adsorbent could uptake As(V) in chemical way with a maximal adsorption capacity of 808.71 mg/g [12]. The compounds composed of M-O bonds have been used as various cations adsorbents. For example, MnO_2 is able to complex with lead (II), copper (II), zinc (II), uranium and Cd(II) [13–15]. It is noteworthy that there are plenty of M-O bonds in the LDHs structure. The bond has extreme potential to complex uranium.

In addition, LDH with unique layered characteristic is a useful raw material to prepare layered double oxides (LDO). LDO yielded from calcining LDH achieves stronger adsorption performance due to (1) sufficient expose of metal atom sites; (2) high specific surface area; and (3) superior scatter than original LDH. LDO thus have gained ascending attention in the fields of catalysis and adsorption. Hong et al. CoMgAl-LDO and CoMgFe-LDO had excellent catalyst performance toward atrazine and carbamazepine because of the expose of three metal atoms [16, 17].

To promote the adsorption capacity of LDH and LDO, much attention has been paid on modification with various chemically foreign objects. For example, Deng et al. increased the congo red adsorption amount of layered double-oxide from 166 mg/g to 344.83 mg/g by coating biochar [18]. Hou et al. calcinated the humic acid loading MgAl-layered double hydroxide into magnetic layered double oxide/carbon. The results proved that the product showed excellent adsorption efficiencies, able to adsorb 386.1 mg/g Cd(II), 359.7 mg/g Pb(II), and 192.7 mg/g Cu(II), respectively [19]. Wu et al. used rare-earth oxides such as La_2O_3, Sm_2O_3, and Er_2O_3 to modify Mg-Al layered double oxides. The consequent material showed higher adsorption-photocatalytic activity toward tetracycline hydrochloride. The removal efficiency reached 99.87% within 110 min under initial TCH concentration of 100 mg/L [20]. Although the post-modification is effective for improving adsorption ability, it introduces other chemical additives and meanwhile increases preparation process step, bringing more pollution and cost.

In the study, two layered double hydroxides (*O*-MgAl-LDHs and *F*-MgAl-LDHs were prepared, where "*O*" and "*F*" denotes oven and freezing processing methods, respectively) and two bimetallic oxides (*O*-MgAl-LDO and *F*-MgAl-LDO) through two processing technique. To our knowledge, there is no detailed data about the adsorption performance relevant with the dry route. The results in the study proved that the freezing process produced larger specific surface area and pore size than the oven process. The difference led to different adsorption performance. Effects of pH, shaking time, ionic strength, initial uranium concentration and temperature on the adsorption of uranium by *O*-MgAl-LDHs, *O*-MgAl-LDO, *F*-MgAl-LDHs and *F*-MgAl-LDO were illustrated. The adsorption mechanism was explained by isotherms, kinetics, thermodynamic models and instrument characteristics.

Materials and methods

Reagents and instruments

Magnesium nitrate ($Mg(NO_3)_2{\cdot}6H_2O$), aluminium nitrate ($Al(NO_3)_3{\cdot}9H_2O$), sodium hydroxide (NaOH), arsenazo III, chloroacetic acid ($ClCH_2COOH$) and anhydrous sodium acetate (CH_3COONa) of analytical grade were received from Aladdin Reagent (Shanghai) Co., Ltd, China and directly used without further purification. The sodium carbonate (Na_2CO_3), sodium bicarbonate ($NaHCO_3$) and nitric acid (68%) of analytical grade were provided by Sinopharm Chemical Reagent Co., Ltd. Triuranium octoxide (U_3O_8) was provided by Quanxin Chemical Industry Co., Ltd.

Scanning electron microscope (SEM) analyses was conducted with Nova Nano SEM 450. The internal structure and crystallinity of layered bimetallic (hydrogen) oxides was recorded using by X-ray diffractometer (D8 ADVANCE). Fourier transform-infrared spectra was obtained using Nicolet-IS10. Surface area and porosity distribution were analyzed using N_2 adsorption-desorption isotherms (ASAP2460). Thermal stability was analyzed by thermogravimetric (TG, Nestal) with a heating rate of 10 ^{o}C/min from room temperature up to 750 ^{o}C. XPS (Thermo ESCALAB 250XI) was used to analyzed the adsorption mechanism.

Preparation of layered bimetallic (hydrogen) oxides

The layered double hydroxide, MgAl-LDHs, was prepared using a modified co-precipitation method [21], which is highly feasible and able to produce a resultant with a uniform internal lattice. In detail, $Mg(NO_3)_2{\cdot}6H_2O$ of 12.82 g and $Al(NO_3)_3{\cdot}9H_2O$ of 3.75 g was dissolved in ultrapure water of 200 mL, followed by addition of the Na_2CO_3-$NaHCO_3$ buffer. The consequent mixture adjusted to pH 7.0 was

stirred for 12 h to make sufficient precipitation reaction. By filtration, the solid product was collected. A part of the solid product was oven-dried at 60 °C for 10 h produce O-MgAl-LDHs. The other was freeze-dried to fabricat F-MgAl-LDHs. The parameters of the freezing-dry were set as the temperature − 78 °C, the pressure 7 Pa and the duration time 10 h. Further calcination at 550 °C transferred O-MgAl-LDHs and F-MgAl-LDHs into the corresponding products, O-MgAl-LDO and F-MgAl-LDO.

Adsorption experiments

The adsorption experiments were conducted with a static batch strategy. In addition, the duplicate parallel experiments were executed to ensure the data no more than 5% relative error. A typcial adsorption operation was as the following. 5.0 mg adsorbent substance (*O*-MgAl-LDHs, *O*-MgAl-LDO, *F*-MgAl-LDHs or *F*-MgAl-LDO) and 50 mL uranium-containing solution of 50 mg/L was mixed in a 250 mL conical flask. Subsequently, the flask was fixed in a thermostatic culture oscillator and oscillated at a constant temperature for a given period. After the adsorption contact, 2.0 mL suspension was taken out and treated by high-speed centrifuge of 9000 r/min. The supernatant was measured to determine the concentration of uranium by a UV-vis spectrophotometry at 660 nm with the standard arsenazo III method. The adsorption amount (mg/g), i.e. the weight of uranium adsorbed onto the adsorbents, was calculated out using Eq. (1)

$$q_e = \frac{(C_0 - C_e)V}{m} \quad (1)$$

where C_0 (mg/L) and C_e (mg/L) are the initial and final uranium concentration, respectively; V (L) is the volume of uranium-containing solution; m (g) is the mass of *O*-MgAl-LDHs, *O*-MgAl-LDO, *F*-MgAl-LDHs or *F*-MgAl-LDO.

Results and discussion

Characterization

Microstructure of *O*-MgAl-LDHs, *O*-MgAl-LDO, *F*-MgAl-LDHs and *F*-MgAl-LDO are displayed in Fig. 1. One can see that layered double hydroxide and bimetallic oxide were heaps of many thin slices. In comparison, F-MgAl-LDHs and F-MgAl-LDO showed petal-shaped structure and more uneven surface than *O*-MgAl-LDHs and *O*-MgAl-LDO. The thermogravimetric data proved O-MgAl-LDH included more moisture content than F-MgAl-LDH. Thus crystalline grains of O-MgAl-LDH tended to form a monoblock, which exposed few active adsorption sites for uranium. On the contrary, F-MgAl-LDH with smaller particle size possessed a larger specific surface area, providing more effective adsorption sites.

Figure 2(a) shows four XRD patterns of layered double hydroxide and bimetallic oxide. Most important of all, the characteristic (003) and (006) peaks of the prepared *O*-MgAl-LDHs and *F*-MgAl-LDHs highly fitting with the standard card $((Mg_4Al_2)(OH)_{12}CO_3{\cdot}3(H_2O))_{0.5}$ (PDF:70-2151) as well as *O*-MgAl-LDO and *F*-MgAl-LDHs and *F*-MgAl-LDO perfectly fitting the standard card MgO (PDF:45–0946) indicated that four bimetallic product were the design compound. In addition, *O*-MgAl-LDHs, *O*-MgAl-LDO, *F*-MgAl-LDHs and *F*-MgAl-LDO were single crystal structure of high purity in view of the narrow and sharp peak.

It can be seen the crystal plane spaces of O-MgAl-LDHs and F-MgAl-LDHs were determined as 8.07 Å and 8.16 Å calculated from D_{003}. The larger plane space of the latter was attributed to the freeze-drying way, in which water molecule left off the solid structure by ice sublimation. Moreover, the average particle size (7.14 nm) of the latter, less than 7.63 nm of the former, proved that the freeze-drying technique resulted in finer particle and larger specific surface area, which was profitable in the adsorption process.

Figure 2(b) shows four FT-IR patterns of layered double hydroxide and bimetallic oxide. The peaks in the wavelength range of 450–735 cm^{-1} observed in *O*-MgAl-LDHs, *O*-MgAl-LDO, *F*-MgAl-LDHs and *F*-MgAl-LDO patters were assigned as M-OH and M-O (M = Al or Mg) lattice vibrations. However, the strong and broad peak at 3550–3735 cm^{-1} well known as hydroxyl groups and the characteristic peak at 1640 cm^{-1} assigned as the bending vibration of interlayer water molecules [22] appeared in *O*-MgAl-LDHs and *F*-MgAl-LDHs patters and disappeared in *O*-MgAl-LDO and *F*-MgAl-LDO patters. The difference was resulted from the the calcination.

The N_2 adsorption-desorption isotherms (Fig. 2c) was used to characterize *O*-MgAl-LDHs, *O*-MgAl-LDO, *F*-MgAl-LDHs and *F*-MgAl-LDO. The type IV isotherm according to the International Union of Pure and Applied Chemistry (IUPAC) classification indicated existance of micropores and mesopores in the prepared substances. Besides, the specific surface area of F-MgAl-LDHs (117.46 m^2/g) is 4.3 times larger than that of O-MgAl-LDHs (27.41 m^2/g). And F-MgAl-LDO has the largest specific surface area (163.15 m^2/g), also bigger than that of O-MgAl-LDHs (88.97 m^2/g). The reason why the freeze-drying process resulted in bigger specific surface area may be that the oven-drying treatment caused structural collapse due to the fierce escape of water molecules while the freeze-drying process had no such adverse influence.

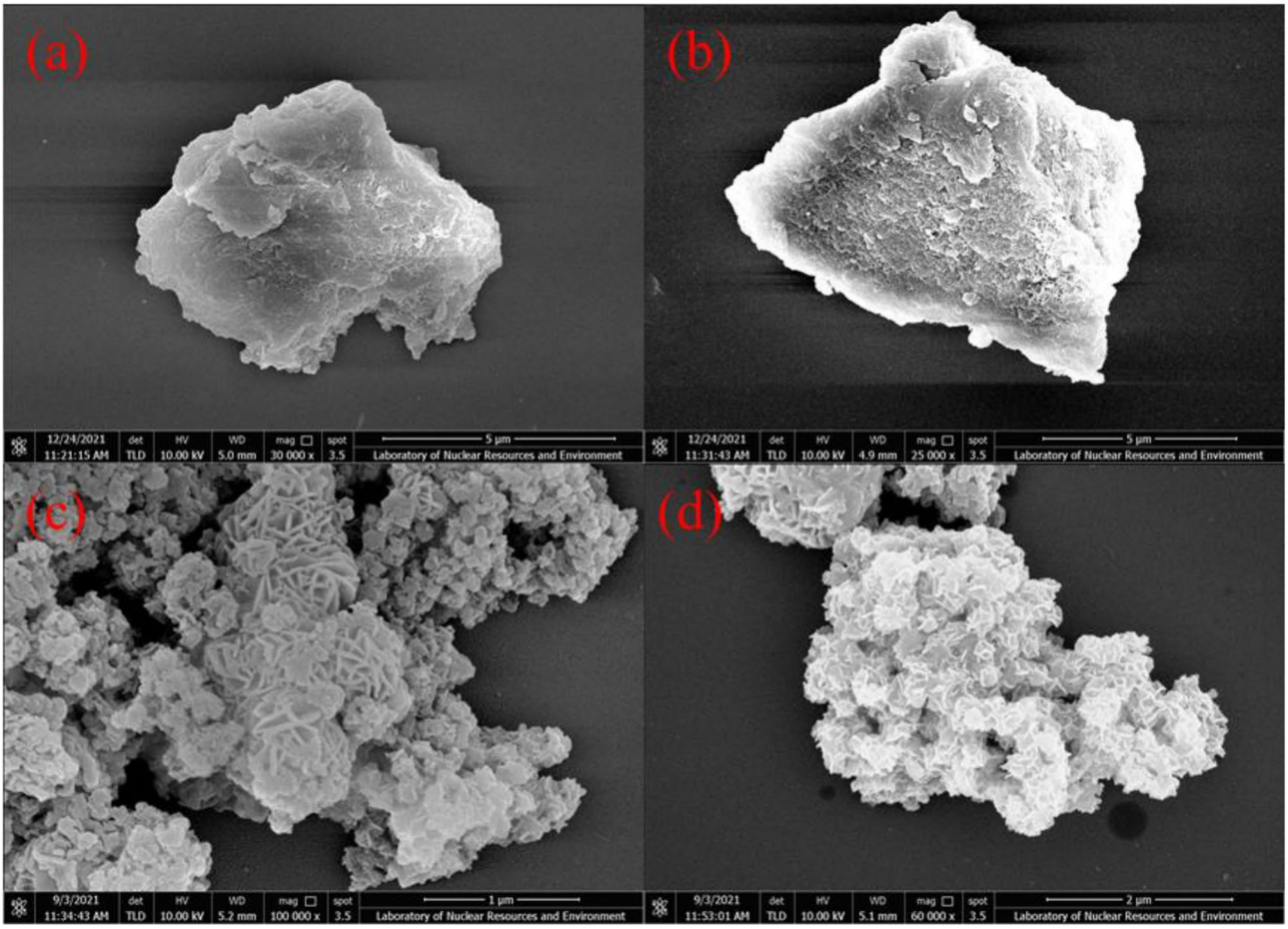

Fig. 1 SEM images of O-MgAl-LDHs (a), O-MgAl-LDO (b), F-MgAl-LDHs (c) and F-MgAl-LDO (d)

The embedded figure in Fig. 2c showed the average pore sizes of O-MgAl-LDHs, O-MgAl-LDO, F-MgAl-LDHs and F-MgAl-LDO were 23.62, 22.47, 25.61 and 23.93 nm, respectively, indicating mesopores pores were dominant.

The mass loss of O-MgAl-LDHs in the first stage (Fig. 2d) was 14.9%, 5.9% higher than that of F-MgAl-LDHs (9.0%), indicating a higher dry extent made by freeze dry. In the second stage, two mass losses were similar, indicating the identical chemistry component. The TG results indicated that the drying method would not vary the main components except moisture content.

Effect of pH and ionic strength

Effect of pH and ionic strength on the adsorption of uranium onto *O*-MgAl-LDHs, *O*-MgAl-LDO, *F*-MgAl-LDHs or *F*-MgAl-LDO were studied (Fig. 3). q_e for *O*-MgAl-LDHs and *O*-MgAl-LDO increased as pH increased from 3.0 to 5.0. Further increase in pH to 7.0 lead to decrease in q_e. Thus the optimal pH for the uranium adsorption by *O*-MgAl-LDHs or *O*-MgAl-LDO were determined as 5.0. The similar tendency were observed for the adsorption by *F*-MgAl-LDHs or *F*-MgAl-LDO except the the optimal pH of 5.5.

Two factors are the main reason for this adsorption phenomenon. (1) One factor is the H^+ concentration in solution, affecting the uranium species distribution (Fig. 3d) and the protonation degree of the adsorbents; (2) The other is surface charge of the adsorbents (Fig. 3c

O-MgAl-LDHs, *O*-MgAl-LDO, *F*-MgAl-LDHs or *F*-MgAl-LDO were positively charged as pH < 5.5 but the charge degree decreased as pH increased. On the other hand, the protonation degree of the adsorbents also declined as pH increased. Both explained q_e plots as pH < 5.0 or 5.5. As pH beyond 5.0, the dominant uranium species was complex state of uranyl, which was not favorable for the adsorption.

The effects of ionic strengths controlled by 0–0.1 M $NaClO_4$ on the uranium adsorption were also studied. One can see that adsorption amount of uranium by MgAl-LDHs and MgAl-LDO were almostly not influenced by the $NaClO_4$ concentration. It can be concluded that uranium uptake onto *O*-MgAl-LDHs, *O*-MgAl-LDO, *F*-MgAl-LDHs or

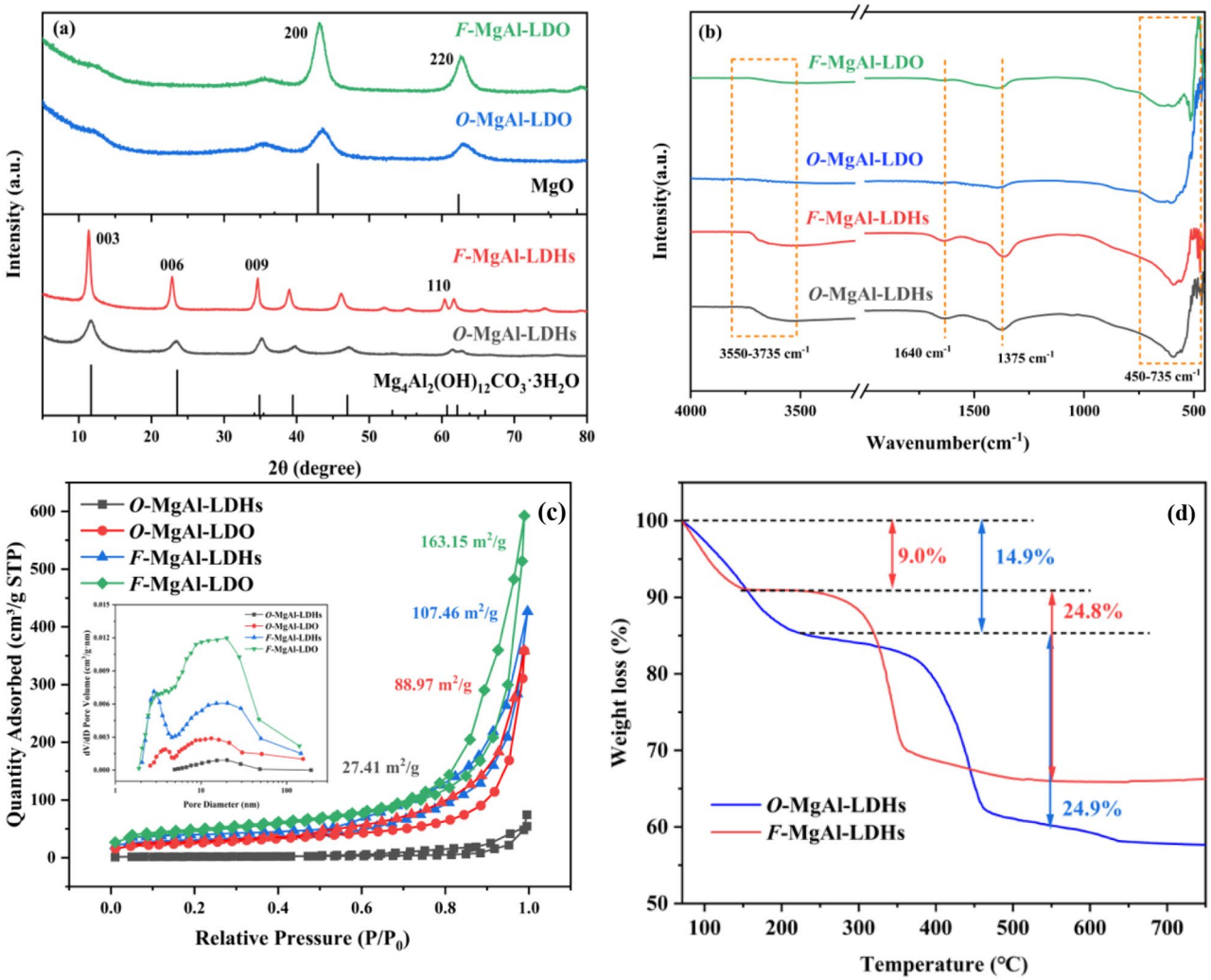

Fig. 2 XRD (a), FT-IR patterns (b), N_2 adsorption-desorption isotherms (c) and TG curves (d)

F-MgAl-LDO were regarded as the inner spherical surface complexation.

Adsorption kinetics

Adsorption kinetics was usually used to judge the adsorption rate and to evaluate the practical application potential of adsorbents. In order to further understand the adsorption process and mechanism of uranyl ions on O-MgAl-LDHs, O-MgAl-LDO, F-MgAl-LDHs and F-MgAl-LDO. The adsorption of uranyl on O-MgAl-LDHs, O-MgAl-LDO, F-MgAl-LDHs and F-MgAl-LDO varying with shaking time were fitted using the pseudo-first-order, pseudo-second-order and intra-particle diffusion model [23], which were expressed as Eq. 2, Eq. 3 and Eq. 4.

$$q_t = q_e(1 - e^{-k_1 t}) \tag{2}$$

$$q_t = \frac{q_e^2 k_2 t}{1 + q_e k_2 t} \tag{3}$$

$$q_t = k_i t^{1/2} + C \tag{4}$$

where q_t (mg/g) and q_e (mg/g) are the uranium adsorption amount of materials at time t and equilibrium, respectively; k_1(min^{-1}), k_2(g/(mg·min)) and k_i(mg/ g·min$^{1/2}$) are the adsorption rate parameters, respectively; C is constant.

The curved fit are conducted in Fig. 4a,b. The calculated parameters are listed in Table 1. One can see that the values of correlation coefficients of the pseudo-second-order model are greater than the values of the Pseudo-first-order and Intra-particle diffusion models. Thus the pseudo-second-order model was appropriative for the reactions between uranyl and O-MgAl-LDHs, O-MgAl-LDO, F-MgAl-LDHs or F-MgAl-LDO, verified by the highest relevant coefficients, 0.991, 0.997, 0.993 and 0.987. Furthermore, the

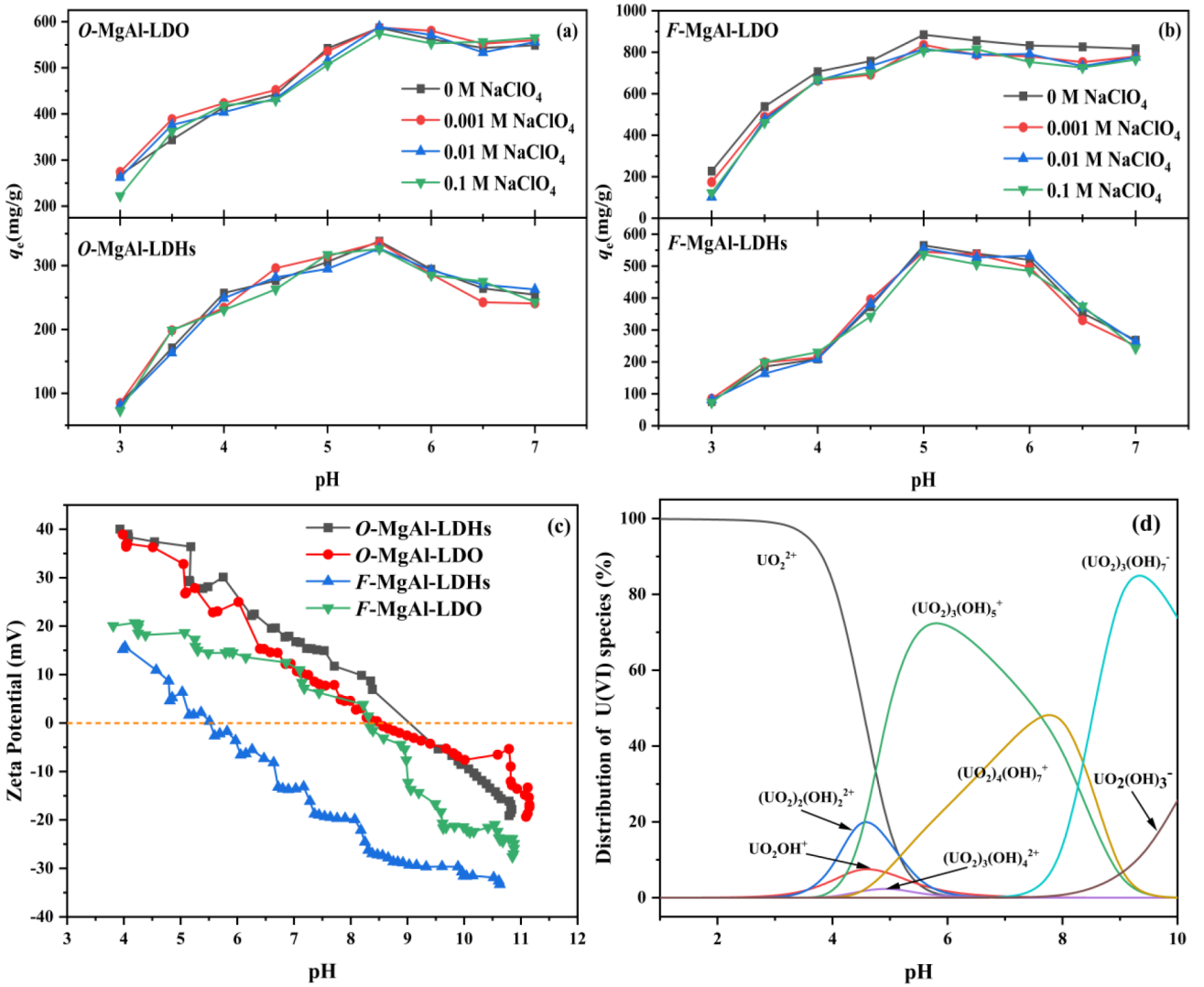

Fig. 3 (a, b) The effect of pH on adsorption under different ionic strengths; (c) Zeta potential; (d) uranium ion form distribution

adsorption amount of uranium on O-MgAl-LDHs, O-MgAl-LDO, F-MgAl-LDHs and F-MgAl-LDO, 347.98 mg/g, 610.90 mg/g, 588.98 mg/g and 968.11 mg/g, respectively determined from pseudo-second-order model were approximate to the experiment values, 338.23 mg/g, 586.97 mg/g, 565.80 mg/g and 882.60 mg/g. Therefore, the adsorption of O-MgAl-LDHs, O-MgAl-LDO, F-MgAl-LDHs and F-MgAl-LDO toward uranyl were identical with the assumption of the pseudo-second-order kinetic model, indicating the adsorption were controlled via chemisorption

Adsorption isotherms

The adsorption isotherm is often used to judge the adsorption nature and to calculate the adsorption capacity. In the study, Langmuir, Freundlich and Dubinin-Radushkevich isotherm models were utilized to fit the isotherm data (Fig. 5).

The Langmuir model (Eq. 5) supposes that the adsorbates adsorbed in the monolayer way on the homogeneous surface of adsorbent [24]. The Freundlich model (Eq. 7) is an empirical relationship describing the quantity of adsorbate on an adsorbent [25]. The Dubinin-Radushkevich isotherm model (Eq. 8) is able to estimate the mean free energy of adsorption [26].

$$q_e = \frac{K_L q_m C_e}{1 + K_L C_e} \tag{5}$$

$$q_e = K_F C_e^{1/n} \tag{7}$$

$$q_e = q_m e^{-K_{DR}\epsilon^2} \tag{8}$$

$$\epsilon = RTln(1 + \frac{1}{C_e}) \tag{9}$$

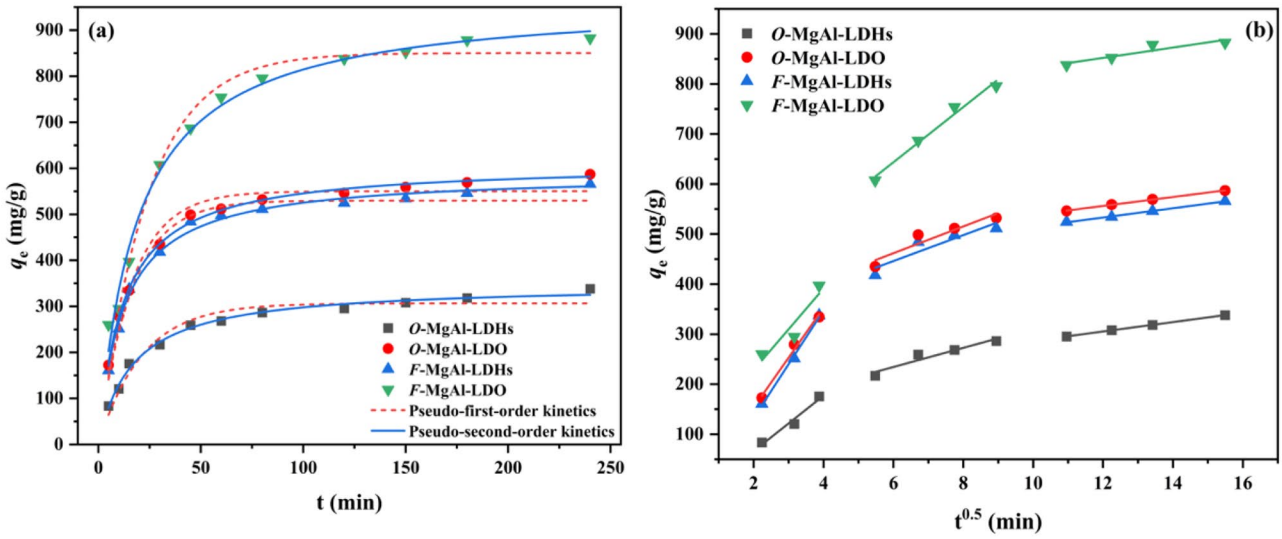

Fig. 4 (a) Effect of time on adsorption and fitting with pseudo-first-order and pseudo-second-order models; (b) Fitting with intra-particle diffusion model

Table 1 Model parameters of pseudo-first-order, pseudo-second-order and intra-particle diffusion

Adsorbents	Pseudo-first-order		
	q_e (mg/g)	k_1 (min^{-1})	R^2
O-MgAl-LDHs	306.63	0.047	0.958
O-MgAl-LDO	550.02	0.062	0.972
F-MgAl-LDHs	529.77	0.062	0.977
F-MgAl-LDO	850.35	0.042	0.974
	Pseudo-second-order		
	q_e (mg/g)	k_2 (g/(mg·min))	R^2
O-MgAl-LDHs	347.98	1.707×10^{-4}	0.991
O-MgAl-LDO	610.90	1.361×10^{-4}	0.997
F-MgAl-LDHs	588.98	1.394×10^{-4}	0.993
F-MgAl-LDO	968.11	5.477×10^{-4}	0.987
	Intra-particle diffusion		
	k_2 (mg/g·$min^{1/2}$)	*C*	R^2
O-MgAl-LDHs	19.18	119.31	0.922
O-MgAl-LDO	26.75	301.33	0.893
F-MgAl-LDHs	25.89	290.79	0.850
F-MgAl-LDO	55.21	312.31	0.981

$$E = \frac{1}{\sqrt{-2K_{DR}}} \tag{10}$$

where q_e (mg/g) and q_m (mg/g) are the adsorption capacity at equilibrium and the maximum adsorption capacity, respectively; C_0 (mg/L) and C_e (mg/L) are the initial and equilibrium uranium concentrations, respectively; K_L (L/mg), K_F[(mg/g) (L/mg)$^{1/n}$] and K_{DR}((mol/kJ)^2) are constants of Langmuir, Freundlich and Dubinin-Radushkevich models, respectively; *n* a characteristic constant related to the adsorption strength; ε (kJ/mol) a constant of the Dubinin-Radushkevich isotherm model. *E* (kJ/mol) is the mean free energy. If *E* value locates between 1.0 and 8.0 kJ/mol, the adsorption is physical; If *E* value belongs to the range of 8.0–16 kJ/mol, the adsorption is chemical in nature [27].

Table 2 listed the parameters' value of three isotherm models above. Higher correlation coefficient R^2 of 0.997, 0.992, 0.996 and 0.997 were achieved via fit the adsorption of O-MgAl-LDHs, O-MgAl-LDO, F-MgAl-LDHs and F-MgAl-LDO with the Langmuir model than that of Freundlich and Dubinin-Radushkevich models. In addition, the theoretical maximum adsorption capacities of O-MgAl-LDHs, O-MgAl-LDO, F-MgAl-LDHs and F-MgAl-LDO calculated by Langmuir model were 476.94 mg/g, 777.91 mg/g, 764.16 mg/g and 1099.93 mg/g, respectively, close to the actual measured results, 406.79 mg/g, 696.04 mg/g, 666.04 mg/g and 1004.55 mg/g. The above fit results proved that the adsorption behavior conformed to the Langmuir assumption. The isotherm fit results demonstrated that the adsorption of uranium onto four adsorbents adopted monolayer way. The uranium adsorption amount of 1099.93 mg/g of F-MgAl-LDO (see the comparation in Table 3) ranked a very competitive position in the uranium specific adsorbents. The outstanding performance verified benefit of the freeze-dry processing for the adsorption.

$$R_L = \frac{1}{1 + K_L C_0} \tag{6}$$

The no-dimensional factor of the Langmuir isotherm model, R_L, can determine the nature of the adsorption process. The adsorption was determined as irreversible adsorption when $R_L = 0$, as favorable adsorption when $0 < R_L < 1$, as linear

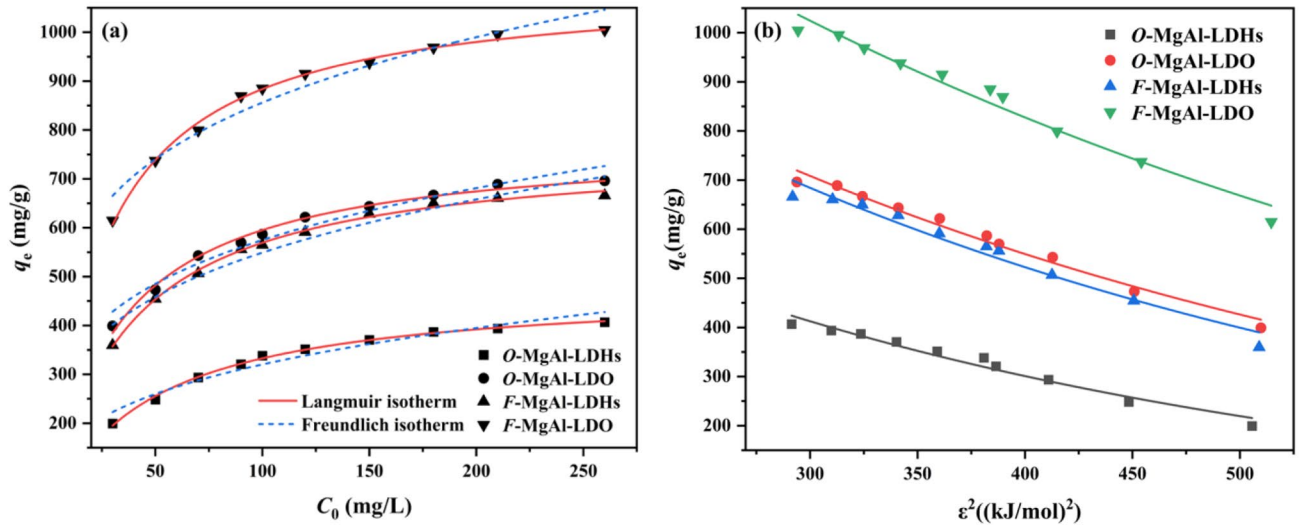

Fig. 5 (a) Effect of initial uranium concentration on adsorption and fitting with Langmuir and Freundlich models; (b) Fitting with Duninin-Radushkevich isotherm model

Table 4 Thermodynamic parameters

	Temperature (K)	ΔG (kJ·mol^{-1})	ΔH (kJ·mol^{-1})	ΔS (J·mol^{-1})	R^2
O-MgAl-LDHs	283	-31.029	-13.947	60.360	0.999
	288	-31.331			
	293	-31.633			
	298	-31.935			
	303	-32.236			
	308	-32.538			
	313	-32.840			
O-MgAl-LDO	283	-30.839	-12.610	64.411	0.995
	288	-31.161			
	293	-31.483			
	298	-31.805			
	303	-32.127			
	308	-32.449			
	313	-32.771			
F-MgAl-LDHs	283	-29.024	-11.823	60.779	0.990
	288	-29.328			
	293	-29.632			
	298	-29.936			
	303	-30.240			
	308	-30.543			
	313	-30.847			
F-MgAl-LDO	283	-71.977	-31.566	142.798	0.936
	288	-72.691			
	293	-73.405			
	298	-74.119			
	303	-74.833			
	308	-75.547			
	313	-76.261			

adsorption when R_L = 1 and as adverse adsorption when

Table 2 Isotherms parameters of Langmuir, Freundlich and Dubinin-Radushkevich models

Adsorbents	Langmuir			
	K_L (L/mg)	q_m (mg/g)		R^2
O-MgAl-LDHs	0.023	476.94		0.997
O-MgAl-LDO	0.033	777.91		0.992
F-MgAl-LDHs	0.029	764.16		0.996
F-MgAl-LDO	0.041	1099.93		0.997
	Freundlich			
	n	K_F ((mg·g^{-1})(L·mg^{-1})$^{1/n}$)		R^2
O-MgAl-LDHs	3.316	79.905		0.948
O-MgAl-LDO	4.089	186.42		0.961
F-MgAl-LDHs	3.836	165.36		0.941
F-MgAl-LDO	4.776	326.40		0.944
	Duninin–Radushkevich			
	q_m (mg/g)	K_{DR} ((mol/kJ)^2) × 10^3	E (kJ/mol)	R^2
O-MgAl-LDHs	1063.06	3.15	12.60	0.965
O-MgAl-LDO	1518.02	2.54	14.03	0.981
F-MgAl-LDHs	1533.91	2.69	13.63	0.962
F-MgAl-LDO	1943.34	2.13	15.32	0.969

R_L >1 [39]. R_L values of the adsorption of O-MgAl-LDHs, O-MgAl-LDO, F-MgAl-LDHs and F-MgAl-LDO are listed in Table 4. All R_L values located between 0 and 1, indicating favorable adsorption.

Effect of temperature

Effect of temperature on the adsorption of uranium on to O-MgAl-LDHs, O-MgAl-LDO, F-MgAl-LDHs and F-MgAl-LDO were investigated. The adsorption

Table 3 The maximal adsorption amount of F-MgAl-LDHs, O-MgAl-LDHs, F-MgAl-LDO, O-MgAl-LDO and some other typical adsorbents

Adsorbent	Experimental conditions	q_{max}(mg/g)	Reference
Titanate/activated carbon	pH = 5.0, T = 298 K	188.00	[28]
Nitrogen-enriched polytriazine	pH = 7.0, T = 298 K	489.00	[29]
Momordica charantia leaf / chitosan	pH = 5.0, T = 303 K	250.70	[30]
Lysinibacillus-GO	pH = 4.5, T = 303 K	149.30	[31]
Arginine-Cellulose	pH = 5.0, T = 298 K	147.00	[32]
Glutamic acid-Cell	pH = 5.0, T = 298 K	168.00	[32]
Polypyrrole	pH = 5.0, T = 298 K	87.72	[33]
Phosphate/Polyethylene	pH = 8.2, T = 298 K	173.80	[34]
ZIF-90-ABOA	pH = 8.0, T = 298 K	353.40	[35]
Aminooxime-ZIF-90	pH = 5.0, T = 298 K	510.60	[36]
Ala-MCS	pH = 6.5, T = 298 K	658.88	[37]
Chitosan/vermiculite/lignin	pH = 4.5, T = 298 K	600	[38]
O-MgAl-LDHs	pH = 5.5, T = 298 K	476.94	This work
O-MgAl-LDO	pH = 5.5, T = 298 K	777.91	This work
F-MgAl-LDHs	pH = 5.5, T = 298 K	764.16	This work
F-MgAl-LDO	pH = 5.5, T = 298 K	1099.93	This work

capacity were obviously influenced by the temperature (Fig. 6). As the temperature rose from 282.5 to 312.5 K, q_e of O-MgAl-LDHs, O-MgAl-LDO, F-MgAl-LDHs and F-MgAl-LDO increased from 274.16 to 400.59 mg/g, 522.98 to 649.71 mg/g, 493.72 to 617.05 mg/g, 827.78 to 949.78 mg/g, indicating a higher temperature were beneficial to the adsorption.

The feasibility and mechanism of the adsorption reactions were evaluated by free energy change (ΔG), enthalpy change (ΔH), and entropy change (ΔS) [40]. The thermodynamic equations are given as the following.

$$K_d = \frac{q_e}{C_e} \tag{11}$$

$$lnK_d = \frac{\Delta S}{R} - \frac{\Delta H}{RT} \tag{12}$$

$$\Delta G = \Delta H - T\Delta S \tag{13}$$

where K_d is the distribution coefficient (L/g), T and R represent the absolute temperature (K) and ideal gas constant (8.314 J/(mol·K)), respectively.

ΔH and ΔS were calculated out by linear fit of ln K_d and $1/T$. The corresponding ΔG at different temperatures were deduced using Eq. 13. Table 3 lists the values of ΔH, ΔS and ΔG. Negative values of ΔH, -13.947 kJ·mol^{-1} for *O*-MgAl-LDHs, -12.610 kJ·mol^{-1} for *O*-MgAl-LDO, -11.823 kJ·mol^{-1} for *F*-MgAl-LDHs, -31.566 kJ·mol^{-1} for *F*-MgAl-LDO meant the adsorption were exothermic. Positive values of ΔS, 60.360 (J·mol^{-1}) for *O*-MgAl-LDHs, 64.411 (J·mol^{-1}) for *O*-MgAl-LDO, 60.779 (J·mol^{-1}) for *F*-MgAl-LDHs, and 142.798 (J·mol^{-1}) for *F*-MgAl-LDO indicated increase in randomness during the adsorption processes. Negative values of ΔG illustrated that the influence of enthalpy changes were less than that of entropy change, revealing adsorption processes were spontaneous at each studied temperature. In addition, the value of ΔG decreasing with the increase in temperature indicated a higher temperature was favorable to the adsorption. The ΔG value of F-MgAl-LDO was significantly less than that of O-MgAl-LDHs, O-MgAl-LDO and F-MgAl-LDHs at the same temperature, highlighting superior uranium adsorption performance.

Table 4 Langmuir isotherm model parameters, R_L (T = 298 K)

Initial uranium concentration (mg/L)	R_L			
	O-MgAl-LDHs	*O*-MgAl-LDO	*F*-MgAl-LDHs	*F*-MgAl-LDO
30	0.606	0.518	0.550	0.464
50	0.478	0.389	0.421	0.339
70	0.390	0.308	0.336	0.264
90	0.334	0.259	0.284	0.219
100	0.321	0.248	0.273	0.210
120	0.274	0.208	0.230	0.175
150	0.236	0.177	0.196	0.147
180	0.204	0.152	0.169	0.126
210	0.180	0.133	0.149	0.110
260	0.151	0.110	0.124	0.091

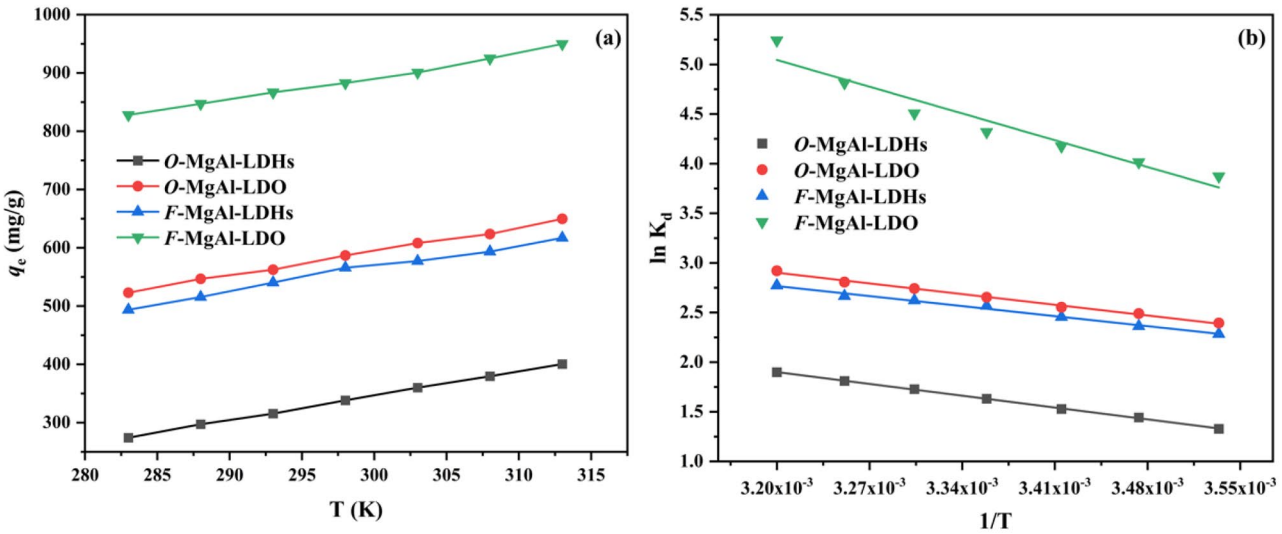

Fig. 6 (a) Effect of temperature on adsorption; (b) Fitting with lnK_d vs. 1/T

Selectivity, elution efficiency and reusability

The freeze-dried F-MgAl-LDHs and F-MgAl-LDO show high adsorption capacity for uranium, which indicates that F-MgAl-LDHs and F-MgAl-LDO have the potential of selective adsorption of uranium. Therefore, a mixed solution containing Ni^{2+}, Co^{2+}, Sr^{2+}, Zn^{2+}, La^{3+}, Gd^{3+}, Ce^{3+}, Sn^{4+} and UO_2^{2+} was treated with F-MgAl-LDHs and F-MgAl-LDO.

Uranium adsorption rates of F-MgAl-LDHs and F-MgAl-LDO in the mixed solution are as high as 84.67% and 96.15%, respectively (Fig. 7). In addition, F-MgAl-LDHs and F-MgAl-LDO have almost no adsorption for Ni, Co, Sr and Zn (less than 10%), suggesting that F-MgAl-LDO has a better selectivity for U(VI) than F-MgAl-LDHs. F-MgAl-LDO has a good selectivity for uranium, probably because its layer spacing matches the diameter of the uranyl ion, keeping the uranyl ion in interlamination.

The elution and reusability of F-MgAl-LDHs and F-MgAl-LDO was conducted by using alkaline solution as the eluent. 0.1 mol/L Na_2CO_3, NaOH and EDTA were able to eluate uranium from the used F-MgAl-LDHs and F-MgAl-LDO (Fig. 7(a)). Of the three eluents, Na_2CO_3 showed the best effectivity, with desorption efficiency of 97.84% and 98.52%, respectively. The possible reason may be that CO_3^{2-} had the most affinity toward uranyl in the three eluents.

Figure 7(b) presents the reusability of F-MgAl-LDHs and F-MgAl-LDO by using Na_2CO_3 as the eluent. The five adsorption-desorption cycles made q_e of F-MgAl-LDO decreases from 882.6 to 534.53 mg/g, a drop about 39.44% and q_e of F-MgAl- LDHs from 565.8 to 285.13 mg/g, a drop about 49.60%. One interesting result should be found that although evident drop were found for both adsorbent, the adsorption capacity were still competitive.

Adsorption mechanism

The FT-IR spectrum of the uranyl loaded F-MgAl-LDHs and F-MgAl-LDO (Fig. S1) exhibited the presence of O = U = O special characteristic peaks at 910 and 911 cm^{-1}, indicating the complexation of the uranyl.

EDS-mapping images of various element distributions are given in Fig. S2. One can see that the distribution of main elements (O, Mg, Al, U) through the F-MgAl-LDHs and F-MgAl-LDO surface was homogeneous.

The atom composition and its surrounding environment of the uranium loading F-MgAl-LDHs and F-MgAl-LDO were studied by XPS. The mechanism of uranium adsorption was therefore deduced. The spectrum in Fig. 8(a) shows that the main elements in F-MgAl-LDHs and F-MgAl-LDO including C, O, Mg and Al, and an obvious U peak, indicating that uranium was adsorbed. The double peaks at 381.3 eV and 392.1 eV with difference of 10.8 eV in Fig. 8(b) was characteristic spectrum of uranium, assigned as U $4f_{7/2}$ and U $4f_{5/2}$, respectively [41].

Overall, the binding energies of C1s, O1s, Mg1s and Al2p increased after interacting F-MgAl-LDHs and F-MgAl-LDO with uranium. This may be because uranium combined with the interlayer anion ($MOCO_2^-$) and metal oxide (M-O) of the material to form $(MOCO_2)_2UO_2^+$ and $(MO)_2UO_2^+$. In detail, O1s binding energy of F-MgAl-LDHs shifted 521.93 eV denoted as O-H bond to 532.13 eV after adsorption, while O1s binding energy of F-MgAl-LDO varied slightly, proving a stronger complex ability of O-H toward uranium [42]. In addition, binding energies of C1s,

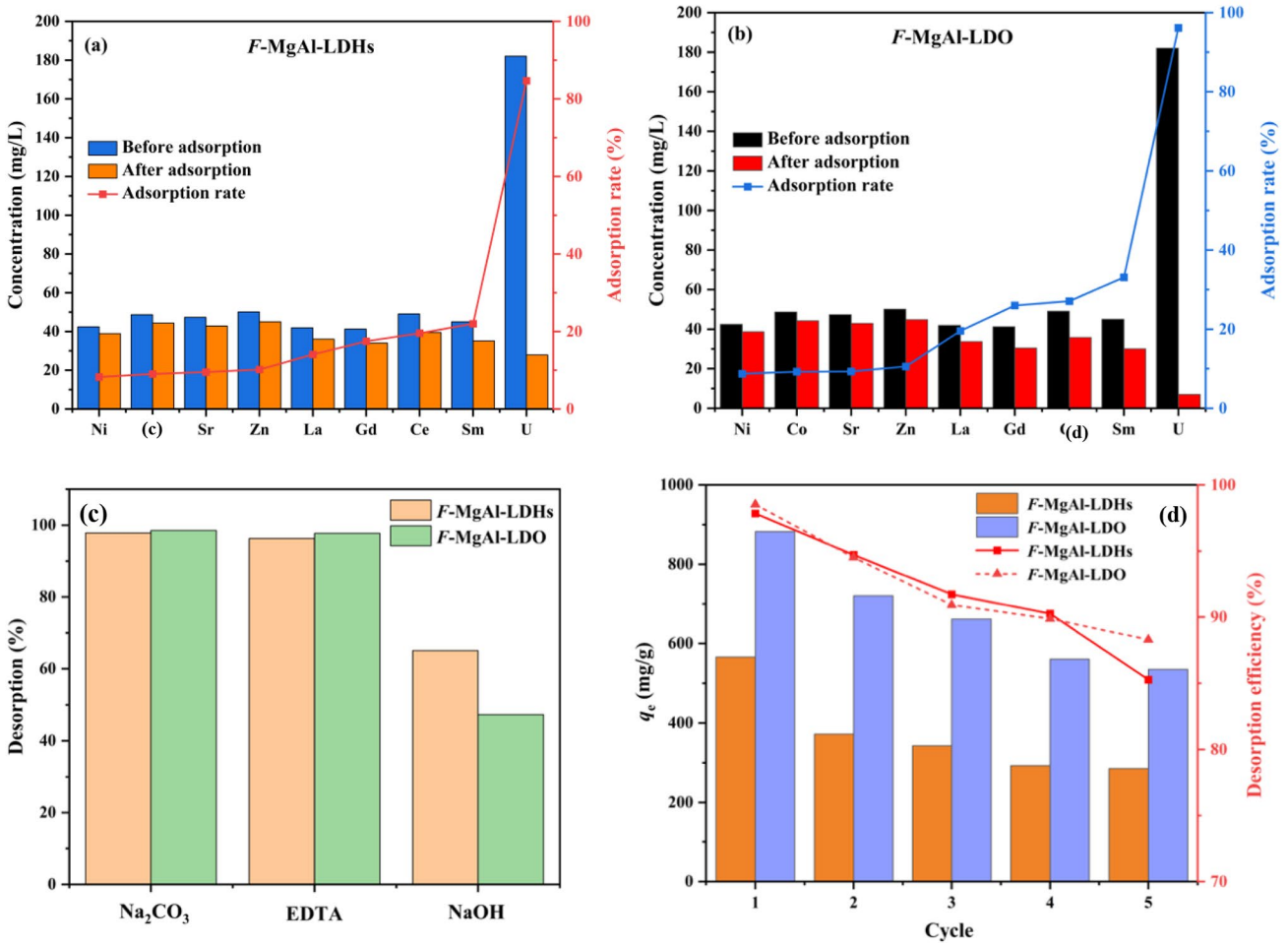

Fig. 7 The effect of coexisting cations on the adsorption on F-MgAl-LDHs (a) and F-MgAl-LDO (b) ; F-MgAl-LDHs and F-MgAl-LDO elution performance (c) and 5 times adsorption-desorption experiments (d)

Mg1s and Al2p (Fig. 8(d,e,f)) increased slightly, illustrating the three atoms indirectly interacted with uranium [43]. Based on the results, the adsorption mechanism could be proposed as Eq. 14 and Eq. 15.

The bond energy of C-O bond in C1s after adsorption also increases (Fig. 8(d)), forming a stable C-O-U bond. The charge density on the C-O and O-H bonds is transferred to the C-C and M-O bonds, resulting in lower bond energies. The adsorption mechanism of uranium by F-MgAl-LDHs and F-MgAl-LDO includes co-precipitation and complexation on the inner surface of the sphere, and the possible complexation reaction is as the following.

$$2MOCO_2^- + UO_2^{2+} \rightarrow (MOCO_2)_2UO_2 \quad (14)$$

$$2MO + UO_2^{2+} \rightarrow (MO)_2UO_2 \quad (15)$$

Conclusion

Mg-Al layered double hydroxides (LDH) (F-MgAl-LDHs and O-MgAl-LDHs) and Mg-Al layered double oxides (LDO) (F-MgAl-LDO and O-MgAl-LDO) nanosheets have been fabricated for the uranium adsorption. The adsorption as functions of pH, initial uranium concentration, contact time, temperature and coexistence ions were illustrated. The main results were as the following: (1) The freeze dry could significant promote the adsorption ability; (2) The optimal pH for the adsorption were at 5.0 ~ 5.5; (3) Of the four materials, the maximum adsorption capacity of F-MgAl-LDO reached 1099.93 mg/g, highlighted the freeze dry as a powerful craft of material process; (4) The adsorption conformed to the assumption of Langmuir and pseudo-second-order model, proving monolayer and chemical adsorption; (5) The adsorption process was spontaneous and endothermic; (6) M-O and C-O bonds participated the complex

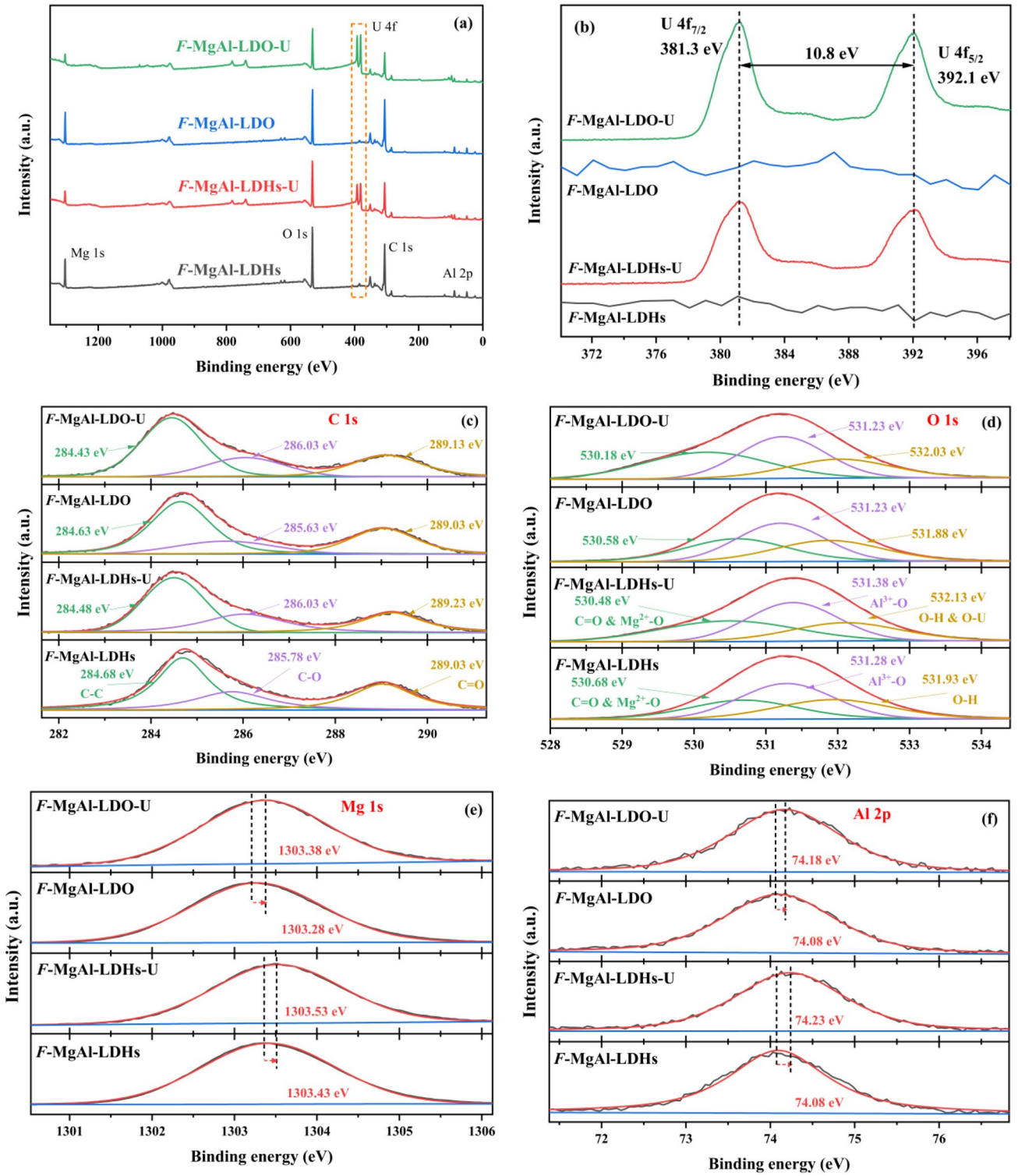

Fig. 8 XPS spectra of F-MgAl-LDHs and F-MgAl-LDO before and after U (VI) adsorption: (a) total spectrum; (b) U 4f; (c) C 1s; (d) O 1s; (e) Mg 1s; (f) Al 2p

process in the uranium adsorption. The results proved qualification of F-MgAl-LDHs, O-MgAl-LDHs, F-MgAl-LDO and O-MgAl-LDO as candidate adsorbents for removal of uranium from wastewater and proposed the freeze dry as an efficient method to promote adsorbent performance.

Acknowledgements This work is financially supported by the National Natural Science Foundation of China (22066001) and the Natural Science Foundation of Jiangxi Province of China (20212ACB213001).

Declarations

Conflict of interest The authors declare that they have no known competing financial interests or personal relationships that could have appeared to influence the work reported in this paper.

References

1. Vasudevamurthy G, Nelson AT (2022) Uranium carbide properties for advanced fuel modeling–A review. J Nucl Mater 558:153145
2. Şenol ZM, Keskin ZS, Özer A, Şimşek S (2022) Application of kaolinite-based composite as an adsorbent for removal of uranyl ions from aqueous solution: kinetics and equilibrium study. J Radioanal Nucl Chem 331:403–414
3. Sar SK, Diwan V, Biswas S, Singh S, Sahu M, Jindal MK, Arora A (2018) Study of uranium level in groundwater of Balod district of Chhattisgarh state, India and assessment of health risk. Hum Ecol Risk Assess 24:691–698
4. Şenol ZM (2021) A chitosan-based composite for adsorption of uranyl ions; mechanism, isothems, kinetics and thermodynamics. Int J Biol Macromol 183:1640–1648
5. Liao J, Liu P, Xie Y, Zhang Y (2021) Metal oxide aerogels: Preparation and application for the uranium removal from aqueous solution. Sci Total Environ 768:144212
6. Ma F, Gui Y, Liu P, Xue Y, Song W (2020) Functional fibrous materials-based adsorbents for uranium adsorption and environmental remediation. Chem Eng J 390:124597
7. Sen K, Mishra D, Debnath P, Mondal A, Mondal NK (2021) Adsorption of uranium (VI) from groundwater by silicon containing biochar supported iron oxide nanoparticle. Bioresour Technol Rep 14:100659
8. Yang L, Chen M, Lu Z, Huang Y, Wang J, Lu L, Cheng X (2020) Synthesis of CaFeAl layered double hydroxides 2D nanosheets and the adsorption behaviour of chloride in simulated marine concrete. Cem Concr Compos 114:103817
9. Wang H, Zhao W, Chen Y, Li Y (2020) Nickel aluminum layered double oxides modified magnetic biochar from waste corncob for efficient removal of acridine orange. Bioresour Technol 315:123834
10. Zubair M, Manzar MS, Mu'azu ND, Anil I, Blaisi NI, Al-Harthi MA (2020) Functionalized MgAl-layered hydroxide intercalated date-palm biochar for Enhanced Uptake of Cationic dye: Kinetics, isotherm and thermodynamic studies. Appl Clay Sci 190:105587
11. Jung KW, Lee SY, Choi JW, Hwang MJ, Shim WG (2021) Synthesis of Mg-Al layered double hydroxides-functionalized hydrochar composite via an in situ one-pot hydrothermal method for arsenate and phosphate removal: structural characterization and adsorption performance. Chem Eng J 420:129775
12. Shi X, Kang L, Hong J, Wang C, Wei R, Naik N, Guo Z (2021) Strong selectivity and high capacity in the adsorption of As (V) from wastewater by glycine-modified Fe/Cu-layered double hydroxides. J Alloys Compd 865:158956
13. Claros M, Kuta J, El-Dahshan O, Michalička J, Jimenez YP, Vallejos S (2021) Hydrothermally synthesized MnO_2 nanowires and their application in Lead (II) and Copper (II) batch adsorption. J Mol Liq 325:115203
14. Sachan D, Das G (2022) Fabrication of Biochar-Impregnated MnO_2 Nanocomposite: Characterization and Potential Application in Copper (II) and Zinc (II) Adsorption. J Hazard Toxic Radioact Waste 26:04021049
15. Ying D, Hong P, Jiali F, Qinqin T, Yuhui L, Youqun W, Zhibin Z, Xiaohong C, Yunhai L (2020) Removal of uranium using MnO_2/orange peel biochar composite prepared by activation and in-situ deposit in a single step. Biomass Bioenergy 142:105772
16. Hong Y, Peng J, Zhao X, Yan Y, Lai B, Yao G (2019) Efficient degradation of atrazine by CoMgAl layered double oxides catalyzed peroxymonosulfate: optimization, degradation pathways and mechanism. Chem Eng J 370:354–363
17. Hong Y, Zhou H, Xiong Z, Liu Y, Yao G, Lai B (2020) Heterogeneous activation of peroxymonosulfate by CoMgFe-LDO for degradation of carbamazepine: Efficiency, mechanism and degradation pathways. Chem Eng J 391:123604
18. Deng H, Li A, Ye C, Sheng L, Li Z, Jiang Y (2020) Green Removal of Various Pollutants by Microsphere Adsorption: Material Characterization and Adsorption Behavior. Energy Fuels 34:16330–16340
19. Hou T, Yan L, Li J, Yang Y, Shan L, Meng X, Li X, Zhao Y (2020) Adsorption performance and mechanistic study of heavy metals by facile synthesized magnetic layered double oxide/carbon composite from spent adsorbent. Chem Eng J 384:123331
20. Wu H, Liu X, Wen J, Liu Y, Zheng X (2021) Rare-earth oxides modified Mg-Al layered double oxides for the enhanced adsorption-photocatalytic activity. Colloids Surf A 610:125933
21. Xu S-d, Dong L, Guo X-y, Wen Y, Jie G (2019) Selenium (VI) removal from caustic solution by synthetic Ca-Al-Cl layered double hydroxides. Trans Nonferrous Met Soc China 29:1763–1775
22. Karami Z, Jouyandeh M, Ali JA, Ganjali MR, Aghazadeh M, Maadani M, Rahn M, Luzi F, Torre L, Puglia D, Saeb MR (2019) Development of Mg-Zn-Al-CO_3 ternary LDH and its curability in epoxy/amine system. Prog Org Coat 136:105264
23. Noli F, Kapashi E, Kapnisti M (2019) Biosorption of uranium and cadmium using sorbents based on Aloe vera wastes. J Environ Chem Eng 7:102985
24. Aniagor CO, Elshkankery M, Fletcher A, Morsy OM, Abdel-Halim E, Hashem A (2021) Equilibrium and kinetic modelling of aqueous cadmium ion and activated carbon adsorption system. Water Conserv Sci Eng 6:95–104
25. Al-Ghouti MA, Da'ana DA (2020) Guidelines for the use and interpretation of adsorption isotherm models: A review. J Hazard Mater 393:122383
26. Xie J, Lv R, Peng H, Fan J, Tao Q, Dai Y, Zhang Z, Cao X, Liu Y (2020) Phosphate functionalized poly (vinyl alcohol)/poly (acrylic acid)(PVA/PAA): an electrospinning nanofiber for uranium separation. J Radioanal Nucl Chem 326:475–486
27. Xie J, Dai Y, Wang Y, Liu Y, Zhang Z, Wang Y, Tao Q, Liu Y (2021) Facile immobilization of NiFeAl-LDHs into electrospun poly (vinyl alcohol)/poly (acrylic acid) nanofibers for uranium adsorption. J Radioanal Nucl Chem 329:1103–1117
28. Duan J, Ji H, Xu T, Pan F, Liu X, Liu W, Zhao D (2021) Simultaneous adsorption of uranium (VI) and 2-chlorophenol by activated carbon fiber supported/modified titanate nanotubes (TNTs/ACF): Effectiveness and synergistic effects. Chem Eng J 406:126752
29. Chaudhary M, Singh L, Rekha P, Srivastava VC, Mohanty P (2019) Adsorption of uranium from aqueous solution as well as seawater conditions by nitrogen-enriched nanoporous polytriazine. Chem Eng J 378:122236
30. Yuvaraja G, Su M, Chen DY, Pang Y, Kong LJ, Subbaiah MV, Reddy GM (2020) Impregnation of magnetic-Momordica charantia leaf powder into chitosan for the removal of U (VI) from aqueous and polluted wastewater. Int J Biol Macromol 149:127–139
31. Zhao C, Liu J, Deng Y, Tian Y, Zhang G, Liao J, Sun Q (2019) Uranium (IV) adsorption from aqueous solutions by microorganism-graphene oxide composites via an immobilization approach. J Clean Prod 236:117624

32. El-Bohy MN, Abdel-Monem YK, Rabie KA, Farag NM, Mahfouz MG, Galhoum AA, Guibal E (2017) Grafting of arginine and glutamic acid onto cellulose for enhanced uranyl sorption. Cellulose 24:1427–1443
33. Abdi S, Nasiri M, Mesbahi A, Khani MH (2017) Investigation of uranium (VI) adsorption by polypyrrole. J Hazard Mater 332:132–139
34. Shao D, Li Y, Wang X, Hu S, Wen J, Xiong J, Marwani H (2017) M. Phosphate-functionalized polyethylene with high adsorption of uranium (VI). Acs Omega 2(7):3267–3275
35. Qin X, Yang W, Yang W, Ma Y, Li M, Chen C, Pan Q (2021) Covalent modification of ZIF-90 for uranium adsorption from seawater. Micropor Mesopor Mat 323:111231
36. Zhao S, Feng T, Feng L, Yan B, Sun W, Luo G, Wang N (2022) Rapid recovery of uranium with magnetic-single-molecular amidoxime adsorbent,Sep. Purif. Technol.120524
37. Li Y, Dai Y, Tao QQ, Gao Z, Xu L (2022) Ultrahigh efficient and selective adsorption of U(VI) with amino acids-modified magnetic chitosan biosorbents: Performance and mechanism. Int J Biol Macromol 214:54–66
38. Şenol ZM, Kaya S, Şimşek S, Katin KP, Özer A, Marzouki R (2022) Synthesis and characterization of chitosan-vermiculite-lignin ternary composite as an adsorbent for effective removal of uranyl ions from aqueous solution: Experimental and theoretical analyses. Int J Biol Macromol 209:1234–1247
39. Meng J, Lin X, Li H, Zhang Y, Zhou J, Chen Y, Shang R, Luo X (2019) Adsorption capacity of kelp-like electrospun nanofibers immobilized with bayberry tannin for uranium (VI) extraction from seawater. RSC Adv 9:8091–8103
40. Skwarek E, Gładysz-Płaska A, Choromańska J, Broda E (2019) Adsorption of uranium ions on nano-hydroxyapatite and modified by Ca and Ag ions. Adsorption 25:639–647
41. Wang X, Cai Y, Han T, Fang M, Chen K, Tan X (2020) Phosphate functionalized layered double hydroxides (phos-LDH) for ultrafast and efficient U (VI) uptake from polluted solutions. J Hazard Mater 399:123081
42. Lyu P, Wang G, Wang B, Yin Q, Li Y, Deng N (2021) Adsorption and interaction mechanism of uranium (VI) from aqueous solutions on phosphate-impregnation biochar cross-linked MgAl layered double-hydroxide composite. Appl Clay Sci 209:106146
43. Chen M, Li S, Li L, Jiang L, Ahmed Z, Dang Z, Wu P (2021) Memory effect induced the enhancement of uranium (VI) immobilization on low-cost MgAl-double oxide: Mechanism insight and resources recovery. J Hazard Mater 401:123447